CHARACTERIZATION OF THERMAL DISPERSION AND WALL EFFECTS IN POROUS MEDIA

Denis Maillet, denis.maillet@ensem.inpl-nancy.frBenoît Fiers,benoit.fiers@ensem.inpl-nancy.fr
Laboratoire d'Energétique et de Mécanique Théorique et Appliquée (LEMTA), Nancy-Université & CNRS
2, avenue de la forêt de Haye, 54500, Vandoeuvre-lès-Nancy, France

Gilles Ferschneider, gilles.ferschneider@ifp.fr
Institut Français du Pétrole-Lyon, BP3, 69360 Solaize, France

Abstract. *Thermal dispersion is the type of heat transfer occuring in a porous medium through which a fluid flows. An application to chemical packed bed reactors is considered here. Both thermal dispersion modeling in such granular porous media (for further design and control) and its experimental characterization are presented in this article. Its first deals with two thermal dispersion modelling problems. The one-temperature model using a single (enthalpic average) temperature corresponding to homogenizetion of the whole medium (fluid and solid phases) is presented first. The corresponding homogenized heat equation requires the knowledge of the coefficients of a thermal dispersion tensor. These dispersion coefficients, that depend on the Darcy velocity, remain constant over the entire porous bed in a plug flow case, if the bed can be considered as a homogeneous porous medium. However, a practical modelling problem occurs near a solid wall, where this assumption is not valid any more in the case of a granular porous medium: higher porosity in that region makes a channeling effect, associated with higher local Darcy velocities, appear. Division of the bed into two homogeneous regions, near wall layer and core region, with a third region corresponding to the solid wall domain, where conjugate transfer can occur, is considered. Semi-analytical solution of the three corresponding heat equations is made possible by the use of two integral transforms (thermal quadrupole modelling: Laplace transformation in time and Fourier transformation in the flow direction here). Simplifications of this three-layer model allows to build a thermal impedance network, where the near-wall layer is represented by a porous channel, with an average Darcy velocity and a time and space varying bulk temperature, two heat transfer coefficients, and a thermal impedance depending explicitly on the velocity distribution. The second part of the article is devoted to thermal characterization of this channeling effect in an academic porous medium (bed of monodisperse glass beads through which air flows) and of its thermal consequences. This is a parameter estimation problem based on the previous two-dimensional three-layer reduced model, where the experimental signal corresponds to thermocouple measurements inside a laboratory bed. The plug flow case, with uniform surface heating (step in time) over part of the solid wall, is considered. A sensitivity study shows that the near wall parameters (thickness, Darcy velocity, heat capaciy, heat transfer coefficients, longitudinal thermal dispersion coefficient) and the core region parameters (thermocouple positions, that are not perfectly known, Darcy velocity) can be divided into three groups depending on the possible prior knowledge on their values. A corresponding Bayesian least squares sum is constructed consequently and Monte Carlo simulations are used to test of the robustness of the proposed estimation technique that depend on hyperparameters, the standard deviations of the prior distributions of the constrained parameters and of the temperature noise. The only fully unconstrained parameter in this estimation process is the near-wall Darcy velocity. Experimental and reconstructed thermograms, with low residuals, are shown. The resulting channeling effect (ratio of near wall to core velocities) depends on the core region Reynolds number and a corresponding correlation is presented. This channeling effect is larger than what is given in the litterature and its thermal consequence deserve to be considered in chemical bed optimization problems .*

Keywords: *thermal dispersion, granular porous media, channeling, wall effect, Bayesian estimation.*

1. INTRODUCTION

Heat transport in a porous medium through which a fluid is flowing is called thermal dispersion. Its applications are numerous and range from classical ones such as fixed bed reactors in chemical engineering or more recent ones such as underground storage of solar energy or use of metal foams for the cooling of electronic circuits. Modelling such type of transfer requires some closer look at the definition of temperature. Strictly speaking, the structure of a porous medium is deterministic: one can consider both flow and heat transfer as pure convection in the fluid phase and pure diffusion in the solid phase. Unfortunately, it is impossible to model heat transfer at this scale, not because of fundamental reasons, but simply because the local morphology of the medium is unknown. Modelling heat transfer in that type of situation requires making the two phase medium continuous, that is *upscaling* its structure, in order to get a continuous *porous* medium characterized by some structural functions (local porosity, specific area, …). The momentum and heat equations have to be revisited consequently, with the introduction of new thermal quantities (Darcy or filtration velocity, dispersion coefficients) that govern a continuous temperature field, see Kaviany (1999) [1]. This upscaling will be presented in section 2, with the introduction of the simplest heat transfer model that can be used for modeling thermal dispersion, the one-temperature model.

2. THE ONE-TEMPERATURE MODEL

Even if more elaborate models exist, see Quintard (1997) [2], the simplest continuous model that can be used to describe thermal dispersion in a porous medium is based on a local mean 'enthalpic' temperature T_H defined at a point P (and for a given time t) in the homogenized medium. This temperature is the space average of the local temperatures at the points P' of the porous medium (P' belonging either to the solid or fluid phase) located inside a sphere of volume V (P, D) of diameter D and centred at P, see Fig.1. This sphere, also called Representative Elementary Volume (R.E.V.), should constitute a representative volume of the porous medium. This mean temperature is a weighted average, the local volumetric heat capacities $\rho c(\mathrm{P}')$ being used as weights (Moyne et al. 2000) [3]:

$$T_H(\mathrm{P}) = \frac{1}{\rho c_t\, V(\mathrm{P},D)} \int_{V(\mathrm{P},D)} \rho c(\mathrm{P}')\, T(\mathrm{P}')\, \mathrm{d}V(\mathrm{P}') = \frac{1}{\rho c_t} \langle H \rangle (\mathrm{P}) \tag{1}$$

where the total local volumetric heat is :

$$\rho c_t(\mathrm{P}) = \langle \rho c_p \rangle (\mathrm{P}) = \varepsilon_f\, \rho c_f + \varepsilon_s\, \rho c_s \tag{2a}$$

and where ε_f and ε_s are the local volume fractions of the fluid (f) and solid (s) phases ($\varepsilon_f + \varepsilon_s = 1$) and ρc_f and ρc_s the corresponding volumetric heat capacities. In the preceding equations, H (P) is the local enthalpy by unit volume: $H(\mathrm{P}) = \rho c(\mathrm{P})\, T(\mathrm{P})$ and $\langle\ \rangle$ is the averaging operator, defined for any space field f by:

$$\langle f \rangle (\mathrm{P}) = \frac{1}{V(\mathrm{P},D)} \int_{V(\mathrm{P},D)} f(\mathrm{P}')\ \mathrm{d}V(\mathrm{P}') \tag{2b}$$

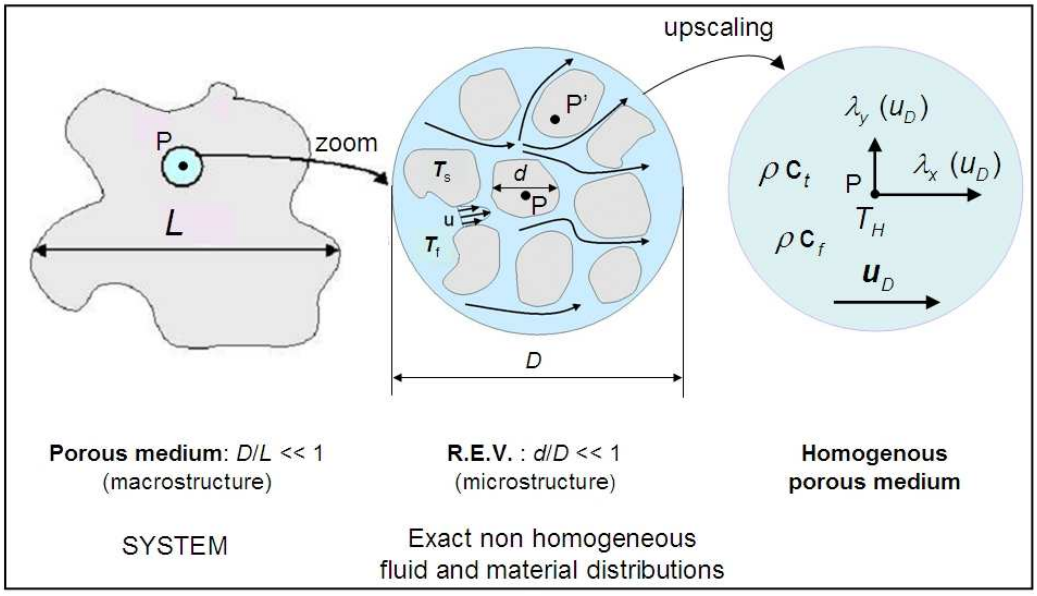

Figure 1. Principle of volume averaging: from two phase porous medium to continuous medium

In the preceding equations time t has not been written as an argument of the different functions, in order to simplify the notation.

Equation (1) can be viewed as a filtering, in the data processing meaning, of the local temperature field, the filter used being a moving average of width D. For this homogenisation to be pertinent, diameter D of the sphere must be much larger than the local characteristic size of the porous medium, here the average diameter d of the grains, and much smaller than the characteristic size L of the system that is modelled, the diameter of the fixed bed reactor for a process engineering application for example.

The local mean temperature T_H used here derives directly from the enthalpic volume average $\langle H \rangle$, which means that it has an energetic meaning. As a consequence, no a priori assumption of local thermal equilibrium is made in its definition and in the use of the reduced one-temperature model that will be presented next.

At this stage it is possible to define a *homogeneous porous medium* as a medium where the local structure does not depend on the location (point *P*, the centre of the Representative Elementary Volume, the sphere shown in Figure 1), characterized by a porosity ε $(=\varepsilon_f)$ that is uniform in the medium.

The one-temperature model requires the definition of a thermal dispersion tensor $\boldsymbol{\lambda}$ whose coefficients can be considered as pseudo-conductivities depending on the nature, thermophysical properties and geometry of the solid grains and of the fluid, as well as on the local Darcy's (or filtration) velocity $\boldsymbol{u}_D$. A convection-diffusion equation for the space and time variations of the averaged temperature can be written for a homogeneous porous medium:

$$\rho c_t \frac{\partial T_H}{\partial t} = \nabla . \left(\boldsymbol{\lambda} \nabla T_H \right) - \rho c_f \ \boldsymbol{u}_D \ . \nabla T_H \ + s \tag{3}$$

with :

$$\boldsymbol{u}_D (P) = \langle \boldsymbol{u} \rangle \tag{4}$$

where $\boldsymbol{u}$ is the local fluid velocity, which is equal to zero in the solid phase.

In this equation, *s* is the volumetric heat rate of a source that can depend on both time and space. One can notice that the coefficient of the transient term is the total volumetric heat ρc_t while the advection term only uses its fluid component ρc_f. The preceding equation (3) can be derived using either the volume averaging technique or the homogenisation method for a spatially periodic porous medium.

3. MODEL FOR CHARACTERIZING THERMAL DISPERSION IN HOMOGENEOUS POROUS MEDIA

In order to characterize experimentally thermal dispersion using the one-temperature model, it is necessary to design an experiment that allows estimation of the unknown parameters present in equation (3) for a homogeneous porous medium: its filtration velocity $\boldsymbol{u}_D$, the principal coefficients $\lambda_x, \lambda_y, \lambda_z$ of the dispersion tensor $\boldsymbol{\lambda}$ and its porosity ε

The simplest type of flow is a plug flow, that is a one-direction flow in the *x* (longitudinal) direction, where the filtration velocity will be noted $u = u_{Dx}$ now on. The longitudinal dispersion coefficient will be called λ_x, while its transverse (or lateral) component (in the direction normal to the flow) will be noted $\lambda_y = \lambda_z$, with the additional assumption of isotropic structure of the medium (no preferential direction).

In order for the porous medium to be uniform, there should not be any wall in the medium, which implies a model (3) valid for a domain of infinite extension in the three directions starting from thermal equilibrium at $T = T_\infty$, where T_∞ is both the initial temperature of the medium, before heating starts, and the temperature of the incoming fluid in the packed bed. Consequently, equation (3) becomes two-dimensional if the heat source $s = s\ (x, y, t)$ is also two-dimensional:

$$\rho c_t \frac{\partial T}{\partial t} = \lambda_x \frac{\partial^2 T}{\partial x^2} + \lambda_y \frac{\partial^2 T}{\partial y^2} - \rho c_f \ u \ \frac{\partial T}{\partial x} + s\ (x, y, t) \tag{5a}$$

The previous model has been used to estimate the two dispersion coefficients in a bed of monodisperse glass beads (d = 2 mm), with either water or air flowing trough it, see Metzger [4] and Testu [5]. Electrical heating by a single resistive wire in the z direction was used. So the source could be written: $s\ (x, y, t) = Q\ \delta(x)\ \delta(y)\ H(t)$, where $\delta(.)$ is the Dirac distribution and H (.) the Heaviside function. In order to prevent any non-linear effect caused by variation with temperature of the different thermophysical properties of both fluid and grains – mass density, viscosity, thermal conductivities – the level of the heat step Q was chosen low enough to get a temperature a rise lower than one Celsius degree. This assumption of constant dispersion coefficients λ_x and λ_y, volumetric heat capacities and filtration velocity makes equation (5a) linear. This equation can be solved using the Green's function technique [4]:

$$T(x,y,t) = \frac{Q}{4\,\pi\,\sqrt{\lambda_x\,\lambda_y}}\;exp\left(\frac{\left(\rho c_p\right)_f u\;x}{2\,\lambda_x}\right)\int_0^{\frac{\left(\rho c_p\right)_f^2 u^2 t}{4\,\left(\rho c_p\right)_t \lambda_x}} exp\left(-\left(\frac{x^2}{\lambda_x}+\frac{y^2}{\lambda_y}\right)\frac{\left(\rho c_p\right)_f^2 u^2}{16\,\lambda_x}\,\frac{1}{\theta}-\theta\right)\frac{d\theta}{\theta} \qquad (5b)$$

This previous model has been used to estimate the two dispersion coefficients in a bed of monodisperse glass beads (d = 2 mm), with either water [4] or air [5] flowing trough it. Internal transient temperature measurements (thermocouples) were inverted using a specific Bayesian estimation that was able to take into account both temperature signal noise as well as uncertainty in the exact location of the thermocouple hot junctions. The correlations corresponding to the longitudinal (x) and lateral (y) dispersion set for air flow through a bed of glass beads are recalled here:

$$\frac{\lambda_x}{\lambda_f} = \frac{\lambda_{eq}}{\lambda_f} + 0.211\,Pe^{1.45} = \frac{\lambda_{eq}}{\lambda_f} + 0.126\,Re^{1.45} \qquad \text{for} \qquad 12 < Re < 130 \quad \text{and} \quad Pr = 0.7 \qquad (6a)$$

$$\frac{\lambda_y}{\lambda_f} = A_y + B_y\,Re = 6.40 + 0.0788\,Re = 6.40 + 0.113\,Pe \quad \text{for } 12 < Re < 130 \quad \text{and} \quad Pr = 0.7 \qquad (6b)$$

where λ_{eq} is the equivalent conductivity of the isotropic equivalent medium composed of fixed solid and fluid phases. Pe (= $u\,d/a_f$, with $a_f = \lambda_f/(\rho c_p)_f$) and Re (= Pe/Pr) are the particulate Péclet and Reynolds numbers. For a bed of glass beads in air, one has λ_{eq} = 0.2 $Wm^{-1}K^{-1}$.

4. NEAR WALL THERMAL EFFECTS

As soon as a solid wall is present in a porous medium, the local structure of the porous medium is modified in its vicinity. This effect is illustrated in Figure 2a for a granular medium used in a chemical reactor (packed bed composed of catalyst grains) through which reactive gases flow: the presence of the reactor walls modify the arrangement of the grains, with a local variation of the porosity: the R.E.V. shown in Figure 1 includes now part of the wall if its center P gets too close to the wall.

The local porosity cannot be calculated with averages (2b) based on a spherical V.E.R. but with surface averages, the surface being for example a disk of diameter d parallel to the wall.

Martin [6] tried to model the consequences of this structure modification on fluid flow and heat and mass transfer in the near-wall region, that cannot be considered as a homogeneous medium anymore. He used the fact that porosity, which is constant in the core region of a bed of spherical beads of diameter d, varies in the near-wall region with the distance to the wall y, as shown in Figure (2b). He proposed the following law in order to model the porosity in the near-wall region:

$$\begin{aligned} &\varepsilon(y) = \varepsilon_{min} + (1-\varepsilon_{min})\,z^2 \qquad \text{if} \quad 0 \le y \le d/2 \\ &\varepsilon(y) = \varepsilon_{core} - (\varepsilon_{core}-\varepsilon_{min})\exp\left(-\frac{1}{4}z\right)\cos\left(\pi\sqrt{\frac{3}{2}}z\right) \qquad \text{if} \quad y \ge d/2 \\ &\text{with} \quad z = 2\,(y/d) - 1 \end{aligned} \qquad (7)$$

where ε_{core} is the porosity of the core region ($y \to \infty$) and ε_{min} the minimum porosity that is met at a distance of one radius from the wall.

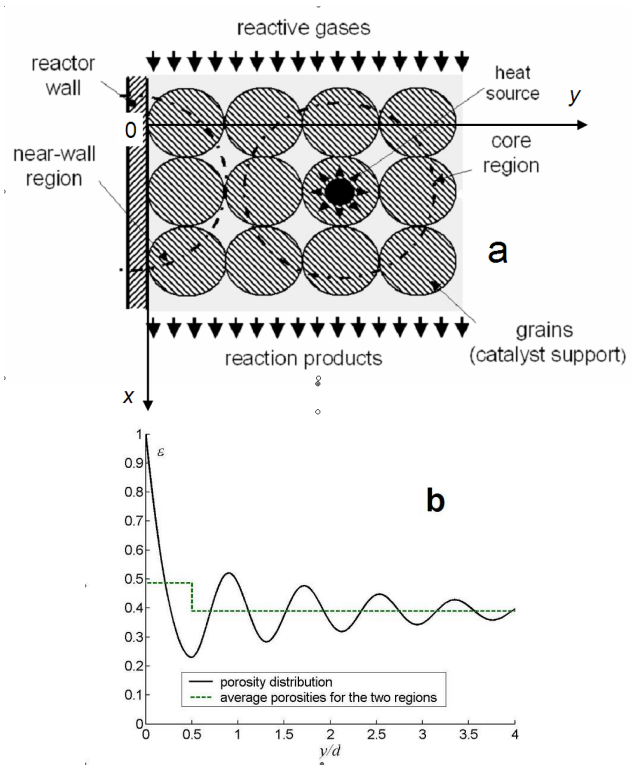

Figure 2. Wall effects: R.E.V. modification (a) and porosity distribution for a packed bed of spheres (b)

The porosity variation with distance to wall is shown in Figure 2b (with $\varepsilon_{core} = 0.39$ and $\varepsilon_{min} = 0.23$). One clearly notices that porosity is maximum at the wall ($\varepsilon = 1$, no solid) and decreases then with damped oscillations that tend to the core porosity ε_∞ for large distances from the wall. If one defines the near-wall region limit by the first minimum of this distribution ($y = \delta = d/2$), it is possible, by averaging equation (3) on the [0 $d/2$] interval, to affect an average porosity $\varepsilon_{near\ wall} = 0.487$ to this region, see Figure 2b.

Martin [6] showed, using Ergun's equation to both parts of the packed bed, that the ratio of these two velocities $\omega = u_{near\ wall} / u_{core}$ depends on the particulate Reynolds number $Re = u_{core}\, d / \nu$.

For very small ($Re \to 0$) or very large ($Re \to \infty$) Reynolds numbers, this ratio takes the asymptotic values $\omega_0 = 2.81$ and $\omega_\infty = 1.53$ respectively (for $\varepsilon_{core} = 0.4$ and $\varepsilon_{near\ wall} = 0.5$). This means that even moderate changes in the porosity distribution will cause considerable flowrate maldistribution with its consequences on the core-to-wall heat transfer.

Studies on the thermal consequences of this channelling effect, see Tsotsas and Schlünder (1988) [7], have shown that the use of an h coefficient was not pertinent to model the wall/bed heat transfer for low Péclet numbers. More recently Winterberg and Tsotsas (2000) [8] proposed to use a lateral dispersion coefficient that varies with the distance to the wall.

5. NON HOMOGENEOUS POROUS MEDIUM REPRESENTATION

5.1 General heterogeneous case

We consider now the configuration depicted in Figure 2a: the volumetric heat source in equation (5) is replaced here by surface heating on the solid wall/porous medium interface, with a surface heat rate $\varphi_{elec}(x,t)$ replacing the volumetric heating s, see Figure 3. Since the porous medium is not homogeneous anymore, its parameters (total volumetric heat, dispersion coefficients) as well as its 1D filtration velocity u (developed flow) are supposed to depend on the distance to the wall y. It is then possible to consider the following heat equation for the enthalpic mean temperature, assuming a zero initial temperature field:

$$\rho c_t(y)\frac{\partial T}{\partial t} = \lambda_x(y)\frac{\partial^2 T}{\partial x^2} + \frac{\partial}{\partial y}\left(\lambda_y(y)\frac{\partial T}{\partial y}\right) - \rho c_f\ u(y)\frac{\partial T}{\partial x} \tag{8}$$

$$-\lambda_y(0)\frac{\partial T}{\partial y} = \varphi_{elec}(x,t) \quad \text{in } y=0\ ; \qquad \text{with : } \quad \varphi_{elec}(x,t) = W\left(H(x) - H(x-\ell)\right)H(t)$$

$$T \to 0 \text{ as } x \to \pm\infty \text{ and } T \to 0 \text{ as } y \to +\infty \quad ; \quad T = 0 \text{ at } t = 0$$

where W is the surface density of the dissipated electrical power.
Functions $u(y)$, $\lambda_x(y)$, $\lambda_y(y)$ and $\rho c_t(y)$ depend on y because ε is a function of y, see equation (7).

5.2 Homogeneous porous medium solution

The first model, noted H1 here, that can be used to simulate heat transfer in this configuration is to suppose the medium homogeneous, that is to pose $\varepsilon = \varepsilon_{core}$ and to consider all the coefficients u, λ_x, λ_y, ρc_t uniform in system (8), see Fig. 5a. In that case, solution of system (8) can be found after an exponential transformation, making the last term of this equation disappear, and a subsequent use of the corresponding Green's function:

$$T(x,y,t) = \frac{W\sqrt{\lambda_x}}{\rho c_f\, u\sqrt{\pi\lambda_y}} \int_0^{\frac{(\rho c_f u)^2 t}{4\rho c_t \lambda_x}} e^{-\frac{(\rho c_f u\, y)^2}{16\,\lambda_x\lambda_y\,\theta}} \left[\operatorname{erf}(z_1) + \operatorname{erf}(z_2)\right]\frac{\mathrm{d}\theta}{\sqrt{\theta}} \tag{9}$$

with:
$$z_1 = \frac{\rho c_f\, u\, x}{4\,\lambda_x\sqrt{\theta}} - \sqrt{\theta} \quad \text{and} \quad z_2 = \frac{\rho c_f\, u\,(\ell - x)}{4\,\lambda_x\sqrt{\theta}} + \sqrt{\theta}$$

An alternate solution can be found through the use of Laplace/Fourier integral transforms (quadrupole method):

$$\overline{T}(x,y,p) = \int_{-\infty}^{+\infty} T(x,y,t)\, exp(-pt)\, \mathrm{d}t \quad ; \quad \overline{\overline{T}}(\alpha,y,p) = \int_{-\infty}^{+\infty} \overline{T}(x,y,p)\, exp(-i\alpha x)\, \mathrm{d}x \tag{10}$$

Heat equation (8), with constant coefficients, becomes, for one layer ($y_1 \le y \le y_2$) of porous medium:

$$\frac{\partial^2 \tilde{\tilde{T}}}{\partial y^2} - \left(\frac{\lambda_x}{\lambda_y}\alpha^2 + \frac{\rho c_2}{\lambda_y} p + i \frac{\rho c_1 u}{\lambda_y}\alpha \right) \tilde{\tilde{T}} = 0 \quad (11)$$

Introducing heat flux $\varphi = -\lambda_y \, \partial T / \partial y$ allows solution of (11) appear in terms of a matrix (quadrupole) relationship between the double transforms of the temperature-transverse flux vector on each face of the layer [8], see Fig. 4a:

$$\begin{bmatrix} \tilde{\tilde{T}} \\ \tilde{\tilde{\varphi}} \end{bmatrix}_{y_1} = \begin{bmatrix} A & B \\ C & D \end{bmatrix} \begin{bmatrix} \tilde{\tilde{T}} \\ \tilde{\tilde{\varphi}} \end{bmatrix}_{y_2} \quad (12)$$

with:

$A = D = \cosh(k e)$; $B = \sinh(k e)/(\lambda_y k)$

$C = \lambda_y k \sinh(k e)$; $k^2 = \frac{\lambda_x}{\lambda_y}\alpha^2 + \frac{\rho c_2}{\lambda_y} p + i \frac{\rho c_1 u}{\lambda_y}\alpha$

An alternate representation, using impedances Z in a "T" analogical network, is possible, see Fig. 4b.

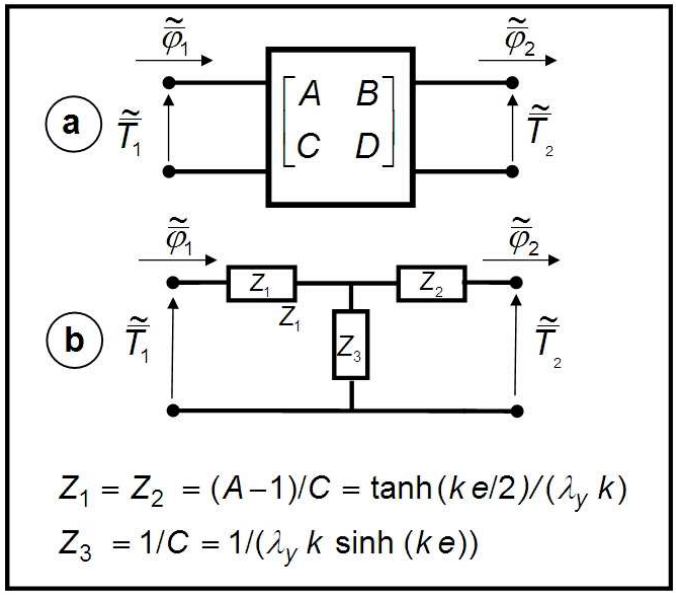

Figure 4. Quadrupole matrix (a) or network (b) representation of one layer of porous material

The alternate solution, equivalent to (5b) is:

$$\tilde{\tilde{T}}_n(y, p) = \frac{e^{-k_n y}}{\lambda_y k_n} \tilde{\tilde{\varphi}}_{n,\text{elec}}(p) \quad \text{with} \quad \alpha_n = n\pi / L \quad (13a)$$

$$\text{and:} \quad \tilde{\tilde{\varphi}}_{n,\text{elec}}(p) = \frac{W}{i p \alpha_n}\left(1 - e^{-i\alpha_n \ell}\right)$$

where L is a large length ($L >> \ell$). The real and imaginary parts of the different $\tilde{T}_n$ modes in the time domain being inverted through a numerical inverse Laplace transform algorithm, see [9]:

$$\tilde{T}_n(y, t) = L^{-1}\left[\tilde{\tilde{T}}_n(y, t) \right] \quad (13b)$$

and return to the space y domain is used with a finite inverse Fourier transform, with a large number N of modes:

$$T(x, y, t) = \frac{1}{L} \sum_{n=-N+1}^{N} \tilde{T}_n(x, t) \exp(i \alpha_n t) \quad (13c)$$

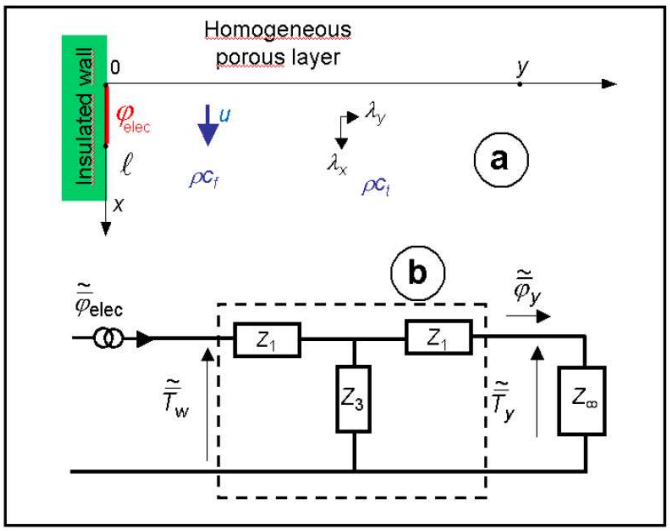

Figure 5. Model H1 – homogeneous porous layer

The analogical representation of the H1 model (13) is shown in Fig. 5b, where the three impedances of the network are:

$$Z_1 = \tanh(k_n y/2)/(\lambda_y k_n) \quad , \quad Z_3 = 1/(\lambda_y k_n \sinh(k_n y)) \quad ; \quad Z_\infty = 1/(\lambda_y k_n) \quad (13d)$$

5.3 Three layer problem

It has been shown above that the presence of a wall made the porous medium non homogeneous. The easiest way to model this heterogeneity is to separate the medium into two homogeneous layers: a near wall layer, of thickness $\delta = d/2$, and porosity $\varepsilon' = \varepsilon_{\text{near wall}}$, and a core region of semi-infinite extent, starting at $y = \delta$, with porosity $\varepsilon = \varepsilon_{\text{core}}$.

The corresponding heat equations are written for each layer:

$$\rho c_t \frac{\partial T}{\partial t} = \lambda_x \frac{\partial^2 T}{\partial x^2} + \lambda_y \frac{\partial^2 T}{\partial y^2} - \rho c_f \, u \frac{\partial T}{\partial x} \qquad \text{for} \qquad \delta \le y \quad (14a)$$

$$\rho c'_t \frac{\partial T'}{\partial t} = \lambda'_x \frac{\partial^2 T'}{\partial x^2} + \lambda'_y \frac{\partial^2 T'}{\partial y^2} - \rho c_f \, u' \frac{\partial T'}{\partial x} \quad \text{for} \quad 0 \le y < \delta \tag{14b}$$

where the prime quantities correspond to the quantities (temperature, uniform filtration velocity, dispersion coefficients, total volumetric heat) of the near wall layer where $\varepsilon' = \varepsilon_{\text{near wall}}$ and the non prime to the core region ($\varepsilon = \varepsilon_{\text{core}}$).

In real experimental situation, conjugated heat transfer in the solid wall (here an anisotropic composite whose thickness is equal to 2*e*): can also be taken into account: the insulation condition at its mid-plane stems from a symmetric arrangement (same porous medium and fluid flow on both side of the plate) to a third heat equation in the solid:

$$\rho c_{\text{wall}} \frac{\partial T_{\text{wall}}}{\partial t} = \lambda_{\text{wall } x} \frac{\partial^2 T_{\text{wall}}}{\partial x^2} + \lambda_{\text{wall } y} \frac{\partial^2 T_{\text{wall}}}{\partial y^2} \quad \text{for} \quad -e \le y \le 0 \tag{14c}$$

System (9a, b, c) must be completed by the boundary, interface and initial conditions:

$$\frac{\partial T_{\text{wall}}}{\partial y} = 0 \ \text{ in } y = -e \quad ; \quad -\lambda_{wall\ y} \frac{\partial T_{\text{wall}}}{\partial y} + \varphi_{\text{elec}}(x,t) = -\lambda'_y \frac{\partial T'}{\partial y} \quad \text{and} \quad T_{\text{wall}} = T' \quad \text{in} \quad y = 0 \tag{10d, e, f}$$

$$T \to 0 \text{ and } T' \to 0 \quad \text{as} \quad x \to \pm\infty ; \ T \to 0 \quad \text{as} \quad y \to +\infty \qquad T' = T \quad \text{and} \quad -\lambda'_x \frac{\partial T'}{\partial y} = -\lambda_x \frac{\partial T}{\partial y} \quad \text{in} \quad y = \delta \tag{14g, h, i, j}$$

$$T = T' = 0 \quad \text{at} \quad t = 0 \tag{14k}$$

The geometry of this new three-layer H3 model is shown in Figure 6a. Analytical solution of the corresponding equations (14a-k) through the use of the Green's functions is not possible anymore, so only the solution in the double transformed domain, see equations (10), will be looked for: each heat equation (14a-c), associated to the boundary or interface equations on the two boundaries of the corresponding domain, can be put under an input/output relationship of the form given by equation (12). Hence, it is possible to make the chain product of the corresponding 2 by 2 matrices, in order to make the interface transformed temperature/flux vectors disappear and to get an analytical solution. The harmonics of order *n* ($n \ge 0$) of the Laplace temperature in the core layer is:

$$\begin{aligned}
&\tilde{\tilde{T}}_n(y,p) = \frac{\exp\left(-k_n(y-\delta)\right)}{\lambda'_n k'_n \sinh(k_n\delta) + \lambda_y k_n \cosh(k_n\delta)} \tilde{\tilde{\varphi}}_{\text{porous } n}(y,p) \qquad \text{if} \quad y \ge \delta \\
&\text{where} \quad \tilde{\tilde{\varphi}}_{\text{porous } n}(y,p) = K_n \, \tilde{\tilde{\varphi}}_{\text{elec } n}(p) \qquad \text{with} \quad K_n = \frac{1}{1+G_n} \\
&\text{and} \quad G_n = \frac{\lambda_{\text{wall } y} \, k_{\text{wall } n} \tanh(k_{\text{wall } n} e)}{\lambda'_n k'_n} \frac{\lambda'_n k'_n \cosh(k_n\delta) + \lambda_y k_n \sinh(k_n\delta)}{\lambda'_n k'_n \sinh(k_n\delta) + \lambda_y k_n \cosh(k_n\delta)} \\
&\text{with} \quad k_n^2 = \frac{\lambda_x}{\lambda_y}\alpha_n^2 + \frac{\rho c_t}{\lambda_y} p + i\alpha_n \frac{\rho c_f \, u}{\lambda_y} \alpha_n \ ; \ k'^2_n = \frac{\lambda'_x}{\lambda'_y}\alpha_n^2 + \frac{\rho c'_t}{\lambda'_y} p + i\alpha_n \frac{\rho c_f \, u'}{\lambda'_y} \ ; \ k^2_{\text{wall } n} = \frac{\lambda_{\text{wall } x}}{\lambda_{\text{wall } y}}\alpha_n^2 + \frac{\rho c_{\text{wall}}}{\lambda_{\text{wall } y}} p
\end{aligned} \tag{15}$$

where φ_{porous} is the flux that enters the porous medium. It is a part of the surface heat source φ_{elec} that is used to electrically heat the system. Coefficient K_n, that is equal to unity in case of a perfectly insulating wall ($\lambda_{\text{wall } y} = 0$), takes into account this type of conjugated transfer between near wall layer and solid wall.

The thermal network of this three-layer system, using Z impedances derived from the four quadrupole matrix coefficients given in Figure 4, are shown in Figure 7b. Here, the three layers thicknesses are the half of the solid plate thickness *e*, the near wall layer thickness δ and the thickness of the core layer between δ and *y*, the point where the transform of temperature, noted T_y here, is looked for. The impedances have the following values:

$$\begin{aligned}
&Z_1 = \tanh\left(k_n (y-\delta)/2\right)/(\lambda_y k_n) \ ; \ Z'_1 = \tanh\left(k'_n \delta/2\right)/(\lambda'_y k'_n) \ ; \ Z_{1\,\text{wall}} = \tanh\left(k_{\text{wall } n} e/2\right)/(\lambda_{\text{wall } y} k_{\text{wall } n}) \\
&Z_3 = 1/\left(\lambda_y k_n \sinh\left(k_n (y-\delta)\right)\right) \ ; \ Z'_3 = 1/\left(\lambda'_y k'_n \sinh\left(k'_n \delta\right)\right) \ ; \ Z_{3\,\text{wall}} = 1/\left(\lambda_{\text{wall } y} k_{\text{wall } n} \sinh\left(k_{\text{wall } n} e\right)\right)
\end{aligned} \tag{16}$$

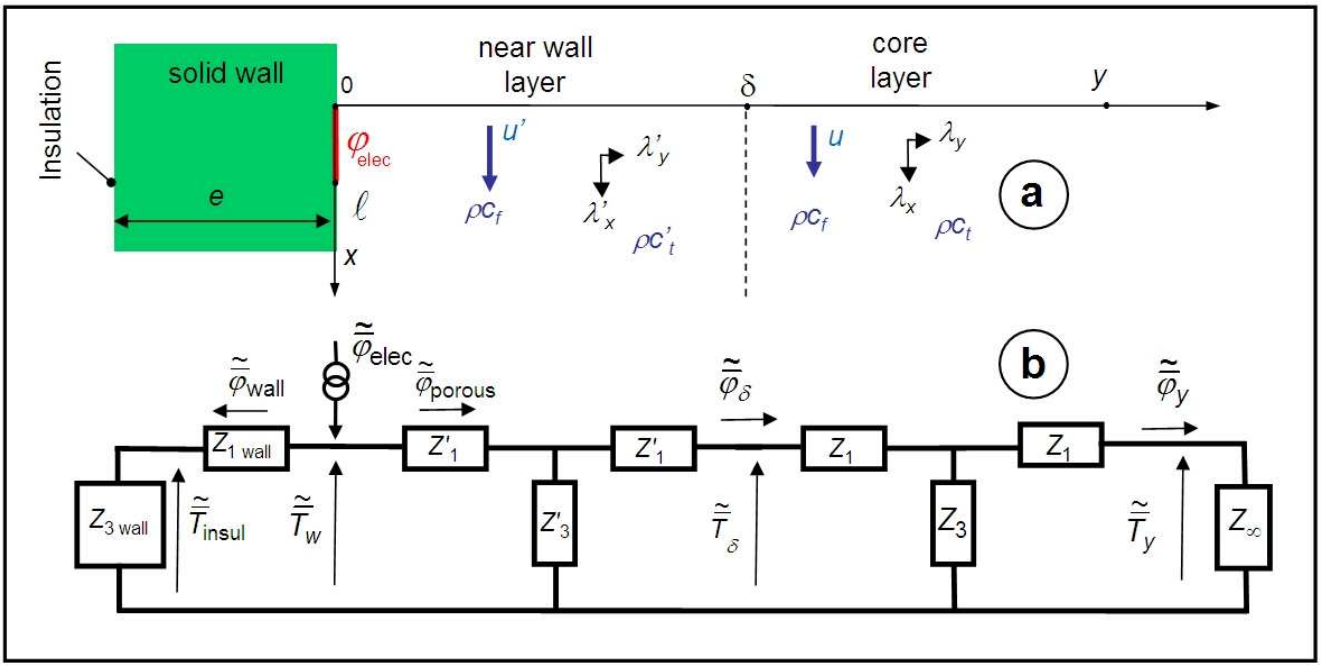

Figure 7. Model H3 – Solid wall/near wall layer/core layer
a) Geometry – b) Analogical thermal network

Let us notice that the temperature field in the core region (15) can also be calculated using the preceding impedances:

$$\tilde{\tilde{T}}_n\ (y,\ p) = \frac{Z'_3}{(1 + Z / Z_\infty)\left[Z_1\ (1/Z + 1/Z_3) + Z'/Z_3\right] + Z_3 / Z}\ \tilde{\tilde{\varphi}}_{\text{porous } n}\ (y,\ p) \quad \text{if} \quad y \geq \delta \tag{16}$$

where $Z = Z_1 + Z_3$ and $Z' = Z'_1 + Z'_3$

In practice, thermal characterization of the wall effects in thermal dispersion requires measurement of transient temperatures inside the porous medium and estimation of the unknown parameters of the model by inversion of these experimental data.

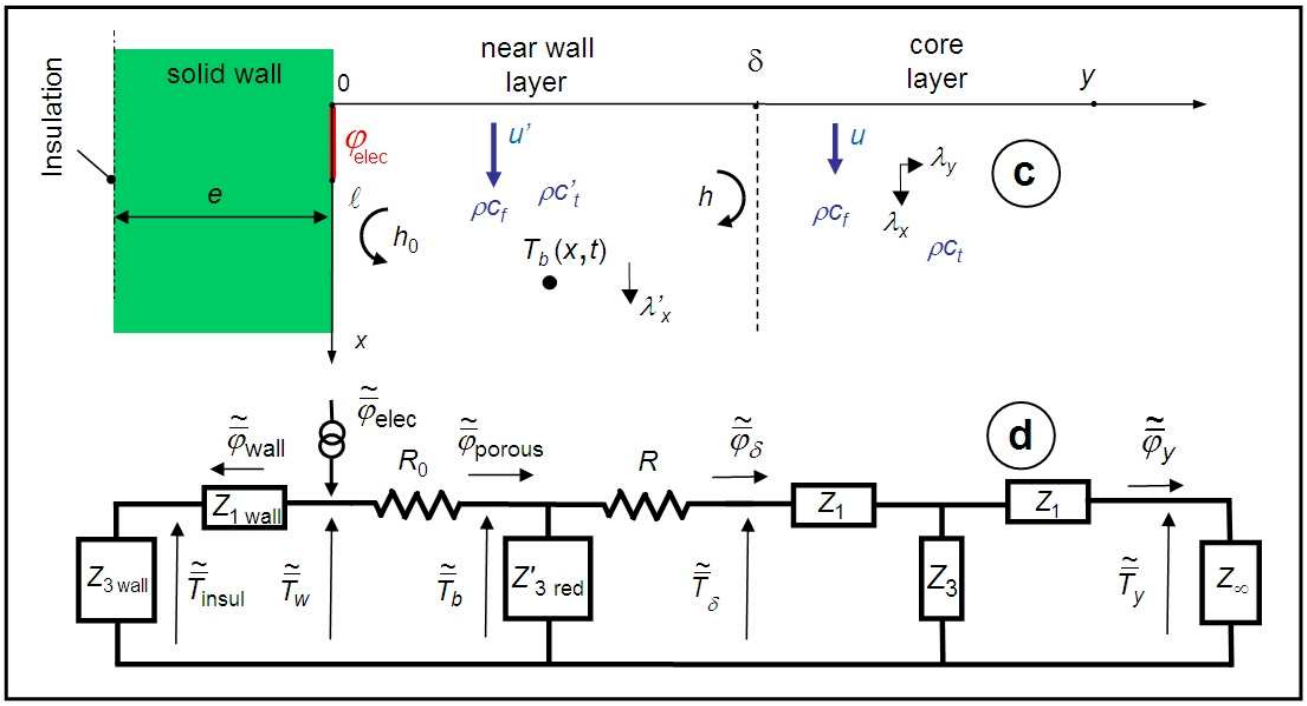

Figure 7. Model H3R – Solid wall/reduced near wall layer/core layer
c) Geometry – d) Analogical thermal network

In practice both velocities *u* and *u'* are unknown, as well as the thermal dispersion coefficients λ'_x and λ'_y and the total volumetric heat $\rho c'_t$ in the near wall layer ($\lambda_x$and λ_y can be calculated by correlation (6), once *u* estimated).

So the difficulties will be large for this experimental estimation, since the parameters being looked for are numerous. Another point deserves to be emphasized: the values of all the parameters of the near wall layer depends also of its thickness δ, here *d*/2, but this value, that can be compared to a boundary layer thickness over a flat plate, is quite arbitrary. So there is no point in making temperature measurement inside the near wall layer and only measurements in the core region deserve to be inverted.

It is therefore possible to reduce the number of parameters of the previous model [10]: the temperature distribution in the near wall layer can be replaced by a unique average temperature over its width, that can be considered as a bulk temperature $T_b(x,t)$ in the corresponding channel of thickness δ and of uniform velocity *u*'. Its Laplace/Fourier transform can be obtained by the corresponding transformations of equation (14b) and by integration over the layer thickness:

$$\tilde{\tilde{T}}_b = Z'_{3\,\mathrm{red}} \left(\tilde{\tilde{\varphi}}_{\mathrm{porous}} - \tilde{\tilde{\varphi}}_{\delta} \right) \text{ with } Z'_{3\,\mathrm{red}} = \frac{1}{\delta \lambda'_y k'^2_n} = \frac{1}{\lambda'_x \delta \alpha_n^2 + \rho c'_t \delta p + i \alpha_n \rho c_f \delta u'} \tag{16}$$

Let us notice here that impedance $Z'_{3\,\mathrm{red}}$ is equal to the first order series expansion of the original "parallel" impedance Z'_3 as δ goes to zero. The physical nature of the three terms of the determination of its expression (16) can be explained:

- $\rho c'_t \delta p$ is a capacitive term that determines the heat amount stored in this channel because of transient effects. It does not play any role for long times (steady state, that is *t* going to infinity or *p* going to zero). Let us note that capacity $\rho c'_t \delta$ incorporates both the fluid and the solid components of the heterogeneous layer;

- $\lambda'_x \delta \alpha_n^2$ is an axial conductance term that causes a *x* redistribution of the local heat flux reaching the porous core layer;

- $i \alpha_n \rho c \alpha_n$ is an axial redistribution term that is caused by advection, that is by the channeling effect (*u'* is larger than *u* for a granular porous medium).

Heat flux entering the porous medium is expressed as: $\varphi_{\mathrm{porous}} = \varphi_{\mathrm{elec}} - \varphi_{\mathrm{wall}}$, where φ_{wall} represents the heat redistributed in the wall with an inertia effect.

Both fluxes $\varphi_{\mathrm{porous}}$ and φ_{wall} have to be related to temperature differences, which is made by replacing the transverse (or lateral) dispersion coefficient λ'_y by two transfer coefficients *h* and h_0:

$$T_{wall}(x,t) - T_b(x,t) = R_0 \ \varphi_{\mathrm{porous}}(x,t) \quad ; \quad T_b(x,t) - T_{\delta}(x,t) = R \ \varphi_{\delta}(x,t) \tag{17a, b}$$

where the two thermal resistances are $R_0 = 1/h_0$ and $R = 1/h$ (on a unit area basis) and φ_{δ} represents the flux that enters the core layer. Let us note, that in the case $h \cong h_0 \cong 2\,\lambda_{eq}/\delta$, these resistances are the first order series expansion of the original "serial" impedance Z'_1 as $k'_n \delta$ goes to zero. An example of steady state temperature distribution, for model H1, for different distances to the wall, is shown in Fig. 8 (air and glass beads, d = 2 mm, ℓ = 10 cm, e = 1 mm, ε = 0.365, ε' = 0.487, N = 2000, L = 3 m). The difference with the H3 model is also plotted: the near wall layer, with its higher velocity, reduces the temperature rise in the core region of the bed.

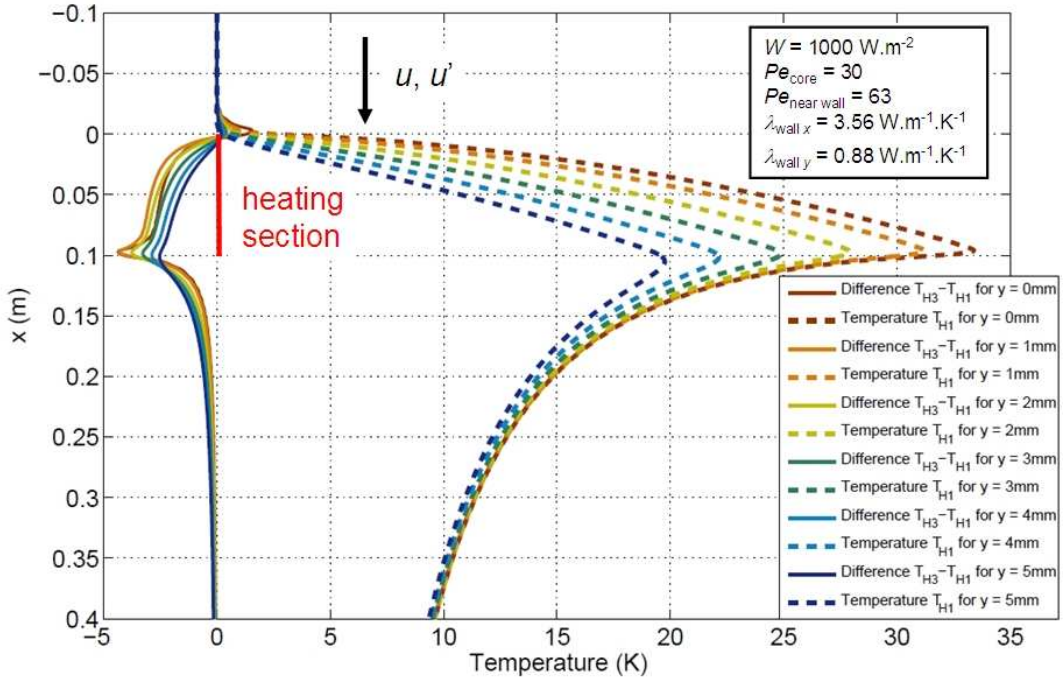

Figure 8. Simulated temperature field for the H1 model (steady state) and comparison with the H3 model

6. EXPERIMENTAL BENCH FOR AND INVERSE METHOD

6.1 Experimental bench

The fixed bed is contained in a polymethyl methacrylate box (150 mm x 200 mm cross section, 400 mm height) with a central plate heated on both of its faces by two foil electrical resistances (in order to guarantee an insulation boundary condition in the *e* mid-plane of the plate, for symmetrical reason) and filled with spherical glass beads with uniform air flow parallel to it. Thermocouples of type E of 127 μm diameter (hot junction of diameters of a few tenth of millimetres) have been embedded in the bed at known (nominal) positions, $(x_i^{\text{nom}}, y_i^{\text{nom}})$, see Fig. 9. Step heating has been applied and the corresponding temperatures have been recorded. Assuming that the thermocouple positions are known, and that the Darcy velocity of the fluid is deduced from the output u_{sensor} of a hot wire sensor in the downstream duct, linking bed and fan, the recorded thermograms can be used to estimate the model parameters.

A sensitivity study (see Fig. 10 further down) showed that parameters of model HR3 are correlated. So external information is needed for their estimation. The experimental bed has been disassembled, and the exact positions of the thermocouples were measured once again: they were slightly different from their original positions. The reason for this deviation is that the glass beads slightly moved the thermocouples when the bed was constructed. So their exact positions always need to be estimated. The same conclusion is valid for the Darcy velocity, because of the inaccuracy of the measuring instrument.

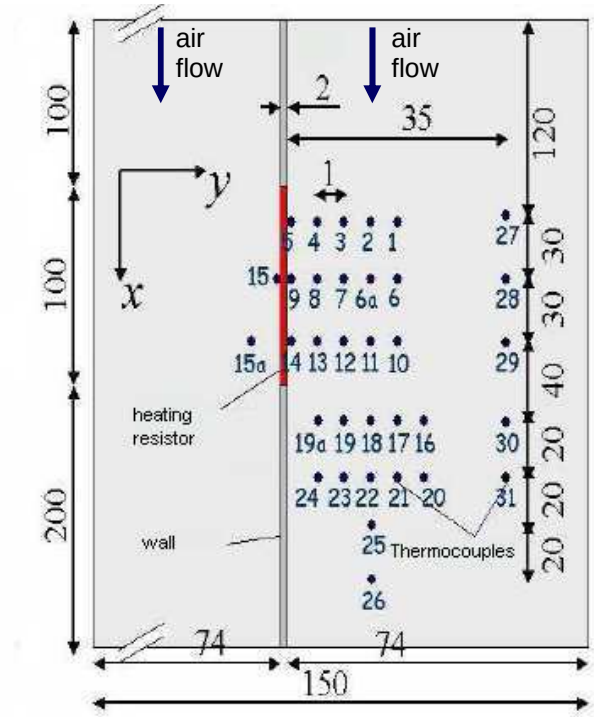

Figure 9. Experimental bench and thermocouple locations

6.2 Sensitivity study and estimation method

Once experimental temperature measurements $T_{ik}^{\exp}$, available at N_s different $(x_i \;\; y_i)$ locations for N_t times t_k, the different parameters β_j, gathered in a column parameter vector $\boldsymbol{\beta}$, can be estimated through minimization of the ordinary least square (OLS) sum:

$$J_{OLS}\ (\boldsymbol{\beta}) = \sum_{i=1}^{Ns} \sum_{k=1}^{Nt} \left(T_{ik}^{\exp} - T\,(x_i, y_i, t_k;\, \boldsymbol{\beta}) \right)^2 = \left\| \boldsymbol{T}^{\exp} - \boldsymbol{T}\,(\boldsymbol{\beta}) \right\|^2 \tag{18}$$

with $\boldsymbol{\beta} = \left[u' \;\; u \;\; ((x_i, y_i), \text{for } i = 1 \text{ to } Ns) \;\; \rho c'_t \;\; h \;\; \delta \right]^T$. So the $n = 6 + 2\,Ns$ parameters present in $\boldsymbol{\beta}$ have to be estimated. In the J_{OLS} sum, the experimental measurements $T_{ik}^{\exp}$ have been put under the form of a single column vector $\boldsymbol{T}^{\exp}$, that is related to the corresponding H3R model output $\boldsymbol{T}\,(\boldsymbol{\beta})$. The difference of these two vectors is equal to the noise vectors where noises ε_{ik} are supposed unbiased (zero expectancy, noted E (.) here), uncorrelated and of constant standard deviation σ_T, with a spherical variance-covariance matrix, noted cov (.) here:

$$\boldsymbol{T}^{\exp} = \boldsymbol{T}\,(\boldsymbol{\beta}) + \boldsymbol{\varepsilon} \qquad \text{where} \quad \mathrm{E}\,(\boldsymbol{\varepsilon}) = \boldsymbol{0}_m \qquad \text{and} \qquad \mathrm{cov}\,(\boldsymbol{\varepsilon}) = \sigma_T^2\ \boldsymbol{I}_m \qquad \text{where} \quad m = Ns \text{ x } Nt \tag{19}$$

Classical non linear minimization techniques, such as the Gauss-Newton method [11], can be used to find the maximum of the least square criterion (18), starting from an initial "guess" corresponding to the nominal values $\boldsymbol{\beta}^{\text{nom}}$ of the different parameters:

$$\boldsymbol{\beta}^{(k)} = \boldsymbol{\beta}^{(k-1)} + \left[\boldsymbol{X}^{\,t}(\boldsymbol{\beta}^{(k-1)})\ \boldsymbol{X}(\boldsymbol{\beta}^{(k-1)}) \right]^{-1} \boldsymbol{X}^{\,t}(\boldsymbol{\beta}^{(k-1)}) \left(\boldsymbol{T}^{\exp} - \boldsymbol{T}\ (\boldsymbol{\beta}^{(k-1)}) \right) \qquad \text{with} \qquad \boldsymbol{\beta}^{(0)} = \boldsymbol{\beta}^{\text{nom}} \tag{20}$$

where $\boldsymbol{X}$ is the sensitivity matrix:

$$\boldsymbol{X}\,(\boldsymbol{\beta}) = \left(\nabla_{\beta}\, \boldsymbol{T}^{\,t} \right)^t = \frac{\mathrm{d}\boldsymbol{T}}{\mathrm{d}\boldsymbol{\beta}} = \begin{bmatrix} \boldsymbol{X}_1^1 & \cdots & \boldsymbol{X}_j^1 & \cdots & \boldsymbol{X}_n^1 \\ \vdots & & \vdots & & \vdots \\ \boldsymbol{X}_1^i & \cdots & \boldsymbol{X}_j^i & & \boldsymbol{X}_n^i \\ \vdots & & \vdots & & \vdots \\ \boldsymbol{X}_1^{Ns} & \cdots & \boldsymbol{X}_j^{Ns} & \cdots & \boldsymbol{X}_n^{Ns} \end{bmatrix} \qquad \text{where} \quad \boldsymbol{X}_j^i = \begin{bmatrix} \boldsymbol{X}_{1j}^i \\ \boldsymbol{X}_{2j}^i \\ \vdots \\ \boldsymbol{X}_{kj}^i \\ \vdots \\ \boldsymbol{X}_{Nt\,j}^i \end{bmatrix} \qquad \text{and} \qquad \boldsymbol{X}_{kj}^i = \left. \frac{\partial T\,(x_i, y_i, t_k;\, \boldsymbol{\beta})}{\partial \beta_j} \right|_{\beta_{q \neq j} = \text{constant}} \tag{21}$$

The coefficients of the reduced sensitivity vectors $\beta_j\, \boldsymbol{X}_{kj}^i$ are plotted, for two fixed location (x_i, y_i), versus time t_k, in Figs. 10a and 10b , for the following values of the parameters: W = 1000 W.m^{-2}, ε = 0.365, ε' = 0.487, u = 0.325 m/s, u'= 0.569 m.s^{-1} (Pe = 30; Pe'= 52.5), λ'_x =1.91Wm^{-1}K^{-1}. For the location (x_i, y_i) parameters, thickness d has been used for normalization and the plotted coefficients are $\delta\, \partial T / \partial x_i$ and $\delta\, \partial T / \partial y_i$. One can notice that sensitivities to the two velocities u and u' are nearly proportional and that sensitivities to x, λ'_x, h are extremely low: it will be necessary to give prior information on the values of these parameters in the criterion to be minimized to prevent a bad conditioning of the information matrix $\boldsymbol{X}^{\,t}\boldsymbol{X}$ that has to be inverted in the minimization algorithm (20). The same remark can be made for the y position whose sensitivity is quite low in the downstream region, see Fig. 10b. Let us note that the volumetric total heat capacity $\rho c'_t$ has a sensitivity that vanishes for long times.

It is therefore possible to distinguish three types of parameters in parameter vector $\boldsymbol{\beta}$:

- parameters with low sensitivity coefficients (λ'_x ,h), or arbitrary values (δ). Choice of their values is not critical. So, they will be considered as "given": $\boldsymbol{\beta}_{\text{given}} = \left[h \;\; \lambda'_x \;\; \delta \right]^t$. During the iterative minimization process, they will be either kept constant equal to their nominal value ($\delta = d/2$) or given by a correlation, see equation (6a) for λ'_x and (6b) for $h = 2\ \delta / \lambda'_y$ = 693 W.m^{-2}.K^{-1}. In practice, we will keep h equal to 1000 W.m^{-2}.K^{-1} further

down.

- parameters whose values should not depart too much from a nominal value β_j^{nom}. These are "supposed to be known": $\boldsymbol{\beta}_{\text{sk}} = \left[u,\ \rho c'_t\ \left((x_i, y_i), \text{for } i = 1 \text{ to } Ns\right)\right]^t$. The nominal values taken here are $u^{\text{nom}} = K\ u_{\text{sensor}}$, where K is the ratio of the areas of the cross sections of the corresponding outlet duct and of the porous bed. $\rho c'_t{}^{\text{nom}}$ is given by equations (2a) and (7) and the nominal values $(x_i^{\text{nom}}, y_i^{\text{nom}})$ corresponding to Fig. 8 are taken for the thermocouple locations. It is compulsory to associate a standard variation that is accepted for the variation of these parameter during the iterative minimization procedure:

- Parameters that are really unknown (no prior information) and whose value entirely depends on the estimation: $\boldsymbol{\beta}_{\text{unknown}} = [u']$. Only an order of magnitude u'_0, depending on u^{nom} through Martin's use of Ergun's equation in the near wall and core layers, see section 4, is available.

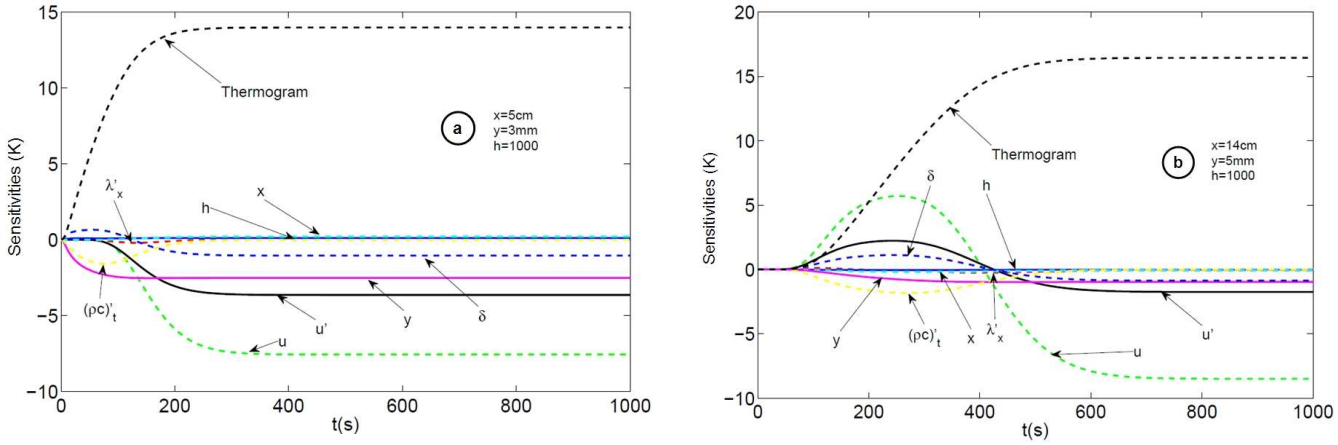

Figure 10. Simulated thermograms and reduced sensitivity coefficients, model H3R

Parameter vector $\boldsymbol{\beta}$ is therefore partitioned into three vectors now:

$$\boldsymbol{\beta} = \begin{bmatrix} \boldsymbol{\beta}_{\text{given}} \\ \boldsymbol{\beta}_{\text{unknown}} \\ \boldsymbol{\beta}_{\text{sk}} \end{bmatrix} \text{ or } \qquad \boldsymbol{\beta} = \begin{bmatrix} \boldsymbol{\beta}_{\text{given}} \\ \boldsymbol{\beta}_{\text{sought}} \end{bmatrix} \qquad \text{with} \qquad \boldsymbol{\beta}_{\text{sought}} = \begin{bmatrix} \boldsymbol{\beta}_{\text{unknown}} \\ \boldsymbol{\beta}_{\text{sk}} \end{bmatrix} \tag{22}$$

which means that only $\boldsymbol{\beta}_{\text{sk}}$ and $\boldsymbol{\beta}_{\text{unknown}}$ will constitute the part $\boldsymbol{\beta}_{\text{sought}}$ of $\boldsymbol{\beta}$ that will be estimated. Let us note that the exact values of the components of both vectors are considered now as stochastic variables. Hence, the constrained OLS sum, that corresponds now to Bayesian estimation [12], becomes:

$$\begin{aligned} J_{\text{Bayes}}(\boldsymbol{\beta}) = \sum_{i=1}^{Ns}\sum_{k=1}^{Nt} \frac{1}{\sigma_T^2}\left(T_{ik}^{\text{exp}} - T(x_i, y_i, t_k; u', u, \rho c'_t, \boldsymbol{\beta}_{\text{given}})\right)^2 + \frac{1}{\sigma_u^2}\left(u - u^{\text{nom}}\right)^2 + \frac{1}{\sigma_{\rho c'_t}^2}\left(\rho c'_t - \rho c'_t{}^{\text{nom}}\right)^2 \\ + \sum_{i=1}^{Ns}\frac{1}{\sigma_x^2}\left(x_i - x_i^{\text{nom}}\right)^2 + \sum_{i=1}^{Ns}\frac{1}{\sigma_y^2}\left(y_i - y_i^{\text{nom}}\right)^2 \end{aligned} \tag{23}$$

Minimization of the new criterion J_{Bayes} criterion can be made using a Gauss-Newton minimization algorithm, similar to (22):

$$\boldsymbol{\beta}_{\text{sought}}^{(k)} = \boldsymbol{\beta}_{\text{sought}}^{(k-1)} + \left[\boldsymbol{X}^t(\boldsymbol{\beta}_{\text{sought}}^{(k-1)})\ \boldsymbol{X}(\boldsymbol{\beta}_{\text{sought}}^{(k-1)}) + \sigma_T^2\ \boldsymbol{R}\ \right]^{-1}\left(\boldsymbol{X}^t(\boldsymbol{\beta}_{\text{sought}}^{(k-1)})\left(\boldsymbol{T}^{\text{exp}} - \boldsymbol{T}(\boldsymbol{\beta}_{\text{sought}}^{(k-1)})\right) + \sigma_T^2\ \boldsymbol{R}\begin{bmatrix} 0 \\ \boldsymbol{\beta}^{\text{nom}} - \boldsymbol{\beta}_{\text{sk}}^{(k)} \end{bmatrix}\right) \tag{24}$$

with $\boldsymbol{\beta}_{\text{sk}}^{(0)} = \boldsymbol{\beta}^{\text{nom}}$

where:

$$\boldsymbol{R} = \begin{bmatrix} 0 & 0 & 0 & \mathbf{0}_{1\,x\,Ns} & \mathbf{0}_{1\,x\,Ns} \\ 0 & \sigma_u^{-2} & 0 & \mathbf{0}_{1\,x\,Ns} & \mathbf{0}_{1\,x\,Ns} \\ 0 & 0 & \sigma_{\rho c'_t}^{-2} & \mathbf{0}_{1\,x\,Ns} & \mathbf{0}_{1\,x\,Ns} \\ \mathbf{0}_{Ns\,x\,1} & \mathbf{0}_{Ns\,x\,1} & \mathbf{0}_{Ns\,x\,1} & \sigma_x^{-2}\boldsymbol{I}_{Ns\,x\,Ns} & \mathbf{0}_{Ns\,x\,Ns} \\ \mathbf{0}_{Ns\,x\,1} & \mathbf{0}_{Ns\,x\,1} & \mathbf{0}_{Ns\,x\,1} & \mathbf{0}_{Ns\,x\,N} & \sigma_y^{-2}\boldsymbol{I}_{Ns\,x\,Ns} \end{bmatrix} \quad \text{with} \quad \boldsymbol{\beta}_{\text{sought}} = \begin{bmatrix} u' \\ u \\ \rho c'_t \\ \boldsymbol{x} \\ \boldsymbol{y} \end{bmatrix} \quad \text{and} \quad \begin{aligned} \boldsymbol{x} &= [x_1 \quad x_2 \quad \cdots \quad x_{Ns}]^t \\ \boldsymbol{y} &= [y_1 \quad y_2 \quad \cdots \quad y_{Ns}]^t \end{aligned}$$

$\boldsymbol{I}_{Ns\,x\,Ns}$ is the identity matrix of size *Ns* x *Ns* and $\mathbf{0}_{p\,x\,q}$ zero matrices of size *p* x *q*.

The different variance ratios, $(\sigma_x / \sigma_T)^2$, $(\sigma_y / \sigma_T)^2$, $(\sigma_{\rho c'_t} / \sigma_T)^2$ and $(\sigma_u / \sigma_T)^2$, can be considered as regularization parameters that allow a compromise between fidelity to the data (minimum of the first term of (23), $J_{OLS}(\boldsymbol{\beta}_{\text{sought}})$, for zero σ_T) and full respect to the constraints ($\boldsymbol{\beta}_{\text{sought}} = \boldsymbol{\beta}^{\text{nom}}$, for σ_x, σ_y, $\sigma_{\rho c'_t}$ and σ_u equal to zero).

6.3 Monte Carlo simulations of inversion

In order to assess the quality of the estimation and to study the effect of the temperature and location noise on the estimator obtained by minimization of sum (23), it is very interesting to implement it on synthesized measurements, that is to use a Monte Carlo process: the exact temperature response of model H3R is noised with an independent additive normal random noise of zero mean and standard deviation σ_T, which yields simulated experimental temperatures T_{ik}^{exp}. The same technique is implemented with both exact thermocouple coordinates (x_i, y_i) that are noised the same way with a noise of standard deviations σ_x and σ_y to produce the nominal locations $(x_i^{\text{nom}}, y_i^{\text{nom}})$. A number N_{simul} = 160 simulations lead to $\hat{\beta}_j^n$ estimates (for j = 1 to N_{simul}) of the j^{th} component of vector $\boldsymbol{\beta}_{\text{sought}}$. Both bias b_j and statistical standard deviations s_j can be calculated for *Ns* = 6 thermocouples:

$$b_j = \overline{\hat{\beta}}_j - \beta_j^{\text{exact}} \qquad \text{and} \qquad s_j = \frac{1}{N_{\text{simul}}} \sum_{n=1}^{N_{\text{simul}}} \left(\hat{\beta}_j^n\right)^2 - \left(\overline{\hat{\beta}}_j\right)^2 \quad \text{with} \quad \overline{\hat{\beta}}_j = \frac{1}{N_{\text{simul}}} \sum_{n=1}^{N_{\text{simul}}} \hat{\beta}_j^n \tag{25a}$$

with the following values of the different standard deviations defining J_{Bayes}:

$$\sigma_T = 0.02 \text{ K} \; ; \; \sigma_x = 1 \text{ mm} \; ; \; \sigma_y = 1 \text{ mm}; \quad \sigma_{\rho c'_t} = 0.05 \; \rho c'^{\,\text{nom}}_t \; ; \quad \sigma_u = 0.20 \; u_{\text{sensor}} \tag{25b}$$

Biases b_j are much lower than standard deviations s_j and the errors e_j (defined as $e_j = |b_j| + s_j$) in the estimated locations were lower than 0.7 mm. Relative errors $e_j / \beta_j^{\text{exact}}$ were 7 % for *u*', 2 % for *u*, and 31 % for $\rho c'_t$.

7. RESULTS

7.1 Thermograms and residuals

In the experimental application [13] of the minimization of J_{Bayes}, a criterion has to be chosen for stopping the iteration. A least square residual sum corresponding to a single measurement was defined:

$$S^{(k)} = (\sigma_T / \sigma_{T\,\text{true}}) \left[J_{\text{Bayes}}(\boldsymbol{\beta}_{\text{sought}}^{(k)}) / (Ns\, Nt) \right]^{1/2} \tag{26}$$

where $\sigma_{T\,\text{true}}$ = 0.01 K is the standard deviation that can be measured before heating starts (this value is twice smaller than the σ_T value used in the definition of J_{Bayes}.

So iterations were stopped as soon as one of the three following criterions were fulfilled: i) $S^{(k)}$ lower than 1.2, ii) ($S^{(k)}$ - $S^{(k-1)}$)/ $S^{(k)}$ lower than 5 10^{-6} and iii) no more than 40 iterations ($k \leq 40$).

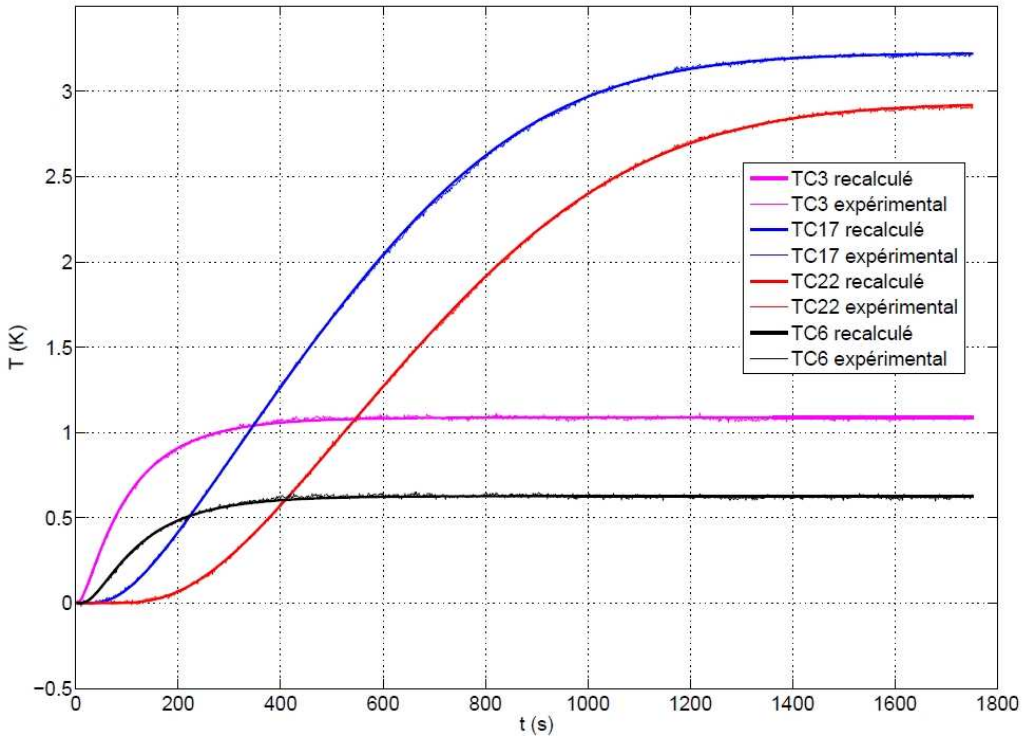

Figure 11. Experimental and recalculated (H3R model) thermograms

Four thermocouples, TC 3 (20 mm, 3 mm), TC 6 (50 mm, 4 mm), TC 17 (120 mm, 4 mm) and TC 22 (140 mm, 4 mm), were chosen for the inversions: two are located in front of the heating plate, at its x level, and the two other ones in the downstream region. The corresponding experimental and recalculated thermograms are shown in Fig. 11. One can see that the residuals are very low. The corresponding values at convergence of the minimization algorithm are: $\hat{u} = 0.115$ m/s; $\hat{u}' = 0.560$ m/s; $\hat{\varepsilon}' = 0.53$; $S = 1.06$.

7.2 Estimation of the channelling effect

The previous estimation technique was applied for core region velocities from 0.06 to 0.511 m/s, which corresponds to core region particulate Péclet numbers in the [6; 48] interval and Reynolds numbers in the [8; 68] interval. The ratio of both estimated average Darcy velocities $\hat{u}'/\hat{u}$ is plotted versus the estimated Péclet number in Fig. 12. One can see that, depending on the velocity and therefore on the Péclet number in the core region of the bed, this velocity ratio is between 2 and 1.5 larger than its value calculated by Martin on the basis of a Ergun law with uniform velocities in the near-wall and core layers (curve also shown in Fig. 12).

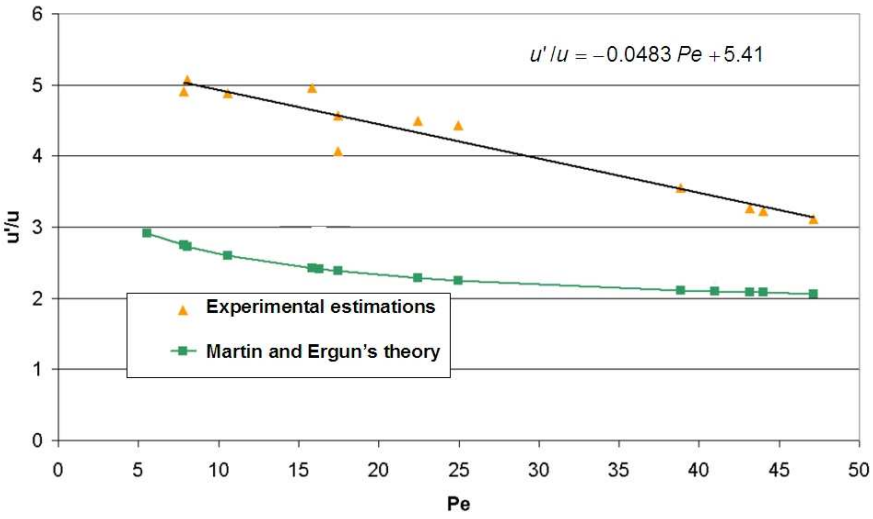

Figure 12. Experimental estimation of the channelling effect

A linear regression has been implemented for our experimental points. It is valid for air flow through a bed of monodisperse spherical beads of core porosity $\varepsilon = 0.365$, with a near-layer thickness δ equal to one bead radius:

$$u'/u = -0.0483Pe + 5.41 = 0.343\ Re + 5.41 \quad \text{for} \quad 6 \le Pe \le 48 \quad \text{and} \quad 8 \le \mathrm{Re} \le 68 \qquad (27)$$

The channeling effect is therefore larger than expected: the maximum temperature deficit in the core of the bed, according to Martin's theory was close to 15 %, see Fig. 8 for a Péclet number equal to 30. This maximum deficit can become larger than 25 % if the same type of simulations is implemented with near-wall layers velocities calculated through equation (27).

8. CONCLUSIONS

The thermal dispersion model that uses only one 'enthalpic' average temperature obtained from an up-scaling process can be used for simulating heat transfer in an air flow through a bed of glass beads. Attention has been brought here to what happens in the region of the bed close to a solid wall. A semi-analytical modelization, in the double Laplace-Fourier transformed domain, allowed to build a thermal impedance network, where the near-wall layer is represented by a porous channel, with an average Darcy velocity and a time and space varying bulk temperature, two heat transfer coefficients, and a thermal impedance depending explicitly on the velocity distribution. Because of this thermal impedance, that takes into account the near-wall layer lower heat capacity and larger velocity and the flux and temperature redistribution in the flow direction caused by longitudinal dispersion in the thickness of this layer, the thermal field in the core region differs from the homogeneous dispersion case.

An experimental bench, with internal point temperature measurements, has been constructed to assess the magnitude of this channelling effect for air flow through a consolidated bed of monodisperse glass beads. It uses a specific Bayesian inverse parameter estimation technique that uses prior information on the thermocouple locations (nominal values) as well as on core velocity (order of magnitude measured by an anemometer) and on the near wall layer heat capacity (theoretical porosity profile). This estimation algorithm, as well as the values of the regularization hyperparameters, have been validated through a Monte Carlo process of inversion of synthesized noised measurements. Experimental inversions using four thermocouple transient temperature measurements and the previous reduced three layer model display very low temperature residuals. They allowed to construct, for different main flow velocities, a correlation giving the velocity ratio (near-wall over core region velocity) as a function of the particulate Reynolds number. This ratio is much higher than what is presented in the literature. As a consequence, channelling effects, for a granular porous medium, affect heat transfer in the core layer of the bed in a higher way than thought previously.

8. REFERENCES

[1] Kaviany, M., 1999, "Principles of heat transfer in porous media", Springer-Verlag ed., New York.
[2] Quintard, M., Kaviany, M., Whitaker, S., 1997, "Two-medium treatment of heat transfer in porous media: numerical results for effective properties", Advances in Water Resources, Vol. 20, pp. 77–94.
[3] C. Moyne, S. Didierjean, H.P. Amaral Souto, O.T. Da Silveira, 2000, "Thermal dispersion in porous media: one-equation Model", Int. J. Heat Mass Transfer 43, 3853–3867.
[4] Metzger, T., Didierjean, S., Maillet, D., 2004, "Optimal experimental estimation of thermal dispersion coefficients in porous media", International Journal of Heat and Mass Transfer, vol. 47, pp. 3341-3353.
[5] Testu, A., Didierjean, S., Maillet, D., Moyne,T., Metzger,T, Niass, T. , 2007, "Thermal dispersion for water or air flow through a bed of glass beads", International Journal of Heat and Mass Transfer, Vol 50, Issues 7-8, 1469-1484.
[6] Martin, H., 1978, "Low Peclet number particle-to-fluid heat and mass transfer in packed beds", Chemical Engineering Science, Vol. 33, pp. 913-919.
[7] Tsotsas, E., Schlünder, E.U.,1988, "Some remarks on channelling and on radial dispersion in packed beds", Chemical Engineering Science, Vol. 43, no5, pp. 1200-1203.
[8] M. Winterberg, M. Tsotsas E. (2000): "Modelling of heat transport in beds packed with spherical particles for various bed geometries and/or thermal boundary conditions". International Journal of Thermal Sciences, Vol. 39, pp.556-572.
[9] Maillet, D., André, S., Batsale, Degiovanni, A., Moyne, C. (2000) "Thermal Quadrupoles – Solving the Heat Equation through Integral transforms". Wiley Ltd Ed., Chichester.
[10] Fiers, B., Testu, A., Maillet, D., Niass, T., 2008, "Wall effects characterization for thermal dispersion in porous media: Importance of a parsimonious parameterization". Journal of Physics: Conference Series. Vol. 135 012041, doi10.1088/1742-6596/135/1/012041.
[11] Beck, J.V., Arnold, K.J., 1977, "Parameter estimation in engineering and science", Wiley, Chichester, U.K.
[12] Kaipio, J., Sommersalo, E., 2005, "Statistical and computational inverse problems", Springer-Verlag, New York, USA.
[13] Fiers, B., Octobre 19, 2009, Thèse de doctorat de l'Institut National Polytechnique de Lorraine, " Transfert de chaleur en proche paroi dans un milieu poreux granulaire. Application aux réacteurs à lit fixe parcouru par un fluide gazeux", in French (doctoral dissertation, "Heat transfer in the near wall region in a granular porous medium. Application to fixed bed reactors with gazeous flow").